Joint CP-AMPA and group I mGlu receptor activation is required for synaptic plasticity in dentate gyrus fast-spiking interneurons

Thomas Hainmüller[a], Kerstin Krieglstein[b], Akos Kulik[c,d], and Marlene Bartos[a,1]

[a]Institute for Physiology I, Systemic and Cellular Neurophysiology, [b]Institute for Anatomy and Cell Biology, Department of Molecular Embryology, [c]Institute for Physiology II, and [d]BIOSS Centre for Biological Signalling Studies, University of Freiburg, 79104 Freiburg, Germany

Edited by Roger A. Nicoll, University of California, San Francisco, CA, and approved August 1, 2014 (received for review May 21, 2014)

Hippocampal principal cell (PC) assemblies provide the brain with a mnemonic representation of space. It is assumed that the formation of cell assemblies is supported by long-lasting modification of glutamatergic synapses onto perisomatic inhibitory interneurons (PIIs), which provide powerful feedback inhibition to neuronal networks. Repetitive activation of dentate gyrus PIIs by excitatory mossy fiber (MF) inputs induces Hebbian long-term potentiation (LTP). In contrast, long-term depression (LTD) emerges in the absence of PII activity. However, little is known about the molecular mechanisms underlying synaptic plasticity in PIIs. Here, we examined the role of group I metabotropic glutamate receptors 1 and 5 (mGluRs1/5) in inducing plastic changes at MF-PII synapses. We found that mGluRs1/5 are located perisynaptically and that pharmacological block of mGluR1 or mGluR5 abolished MF-LTP. In contrast, their exogenous activation was insufficient to induce MF-LTP but cleared MF-LTD. No LTP could be elicited in PIIs loaded with blockers of G protein signaling and Ca^{2+}-dependent PKC. Two-photon imaging revealed that the intracellular Ca^{2+} rise necessary for MF-LTP was largely mediated by Ca^{2+}-permeable AMPA receptors (CP-AMPARs), but less by NMDA receptors or mGluRs1/5. Thus, our data indicate that fast Ca^{2+} signaling via CP-AMPARs and slow G protein-mediated signaling via mGluRs1/5 converge to a PKC-dependent molecular pathway to induce Hebbian MF-LTP. We further propose that Hebbian activation of mGluRs1/5 gates PIIs into a "readiness mode" to promote MF-LTP, which, in turn, will support timed PII recruitment, thereby assisting in PC assembly formation.

hippocampus | parvalbumin | basket cell | GPCR

Reorganization of hippocampal principal cell (PC) assemblies during spatial learning is supported by the timed recruitment of GABAergic cells, specifically parvalbumin (PV)-expressing perisomatic inhibitory interneurons (PIIs) (1, 2). Dentate gyrus (DG) PIIs are excited by glutamatergic granule cells (GCs) via mossy fiber (MF) synapses, which can undergo activity-dependent synaptic plasticity (3, 4). Indeed, after long-term potentiation (LTP), a single MF input can reliably activate PIIs (4), indicating that MF-LTP may influence spatial representation in the DG (2, 5).

Hebbian MF-PII LTP requires precisely timed pre- and postsynaptic activity (4). It is induced in the PII but is expressed presynaptically (3). MF-LTP requires strong intracellular Ca^{2+} elevation and activation of Ca^{2+}-permeable AMPA receptors (CP-AMPARs), but, in contrast to Hebbian LTP at CA1 PII inputs (6), it is independent of NMDA receptors (NMDARs) (4), suggesting that CP-AMPARs could provide the required Ca^{2+} rise for plasticity induction (7, 8). However, recent investigations have proposed a role for group I metabotropic glutamate receptors (mGluRs) in the induction of CP-AMPAR–dependent interneuron plasticity (9–13). Indeed, a Hebbian form of CP-AMPAR–dependent LTP at glutamatergic synapses onto somatostatin (SOM)-expressing CA1 stratum oriens/alveus (O/A) interneurons and at MF inputs onto CA3 interneurons requires mGluR1α activation (9, 11). Furthermore, mGluR1α and mGluR5 contribute to LTP at PC inputs on O/A interneurons, including oriens-lacunosum/moleculare (O-LM) cells (10), but induce long-term depression (LTD) in CA1 fast-spiking GABAergic cells (12). Whether mGluRs1/5 are expressed in hippocampal PV-PIIs remained controversial (14, 15), and their contribution to plasticity in PV-PIIs is unknown. Using whole-cell recordings of GCs paired to PV-PIIs and quantitative immunoelectron microscopy, we show that mGluRs1α/5 are expressed in DG PV-PIIs, contribute to Hebbian LTP, and suppress LTD at their MF inputs. Two-photon (2P) imaging further revealed the main Ca^{2+} sources and Ca^{2+}-mediated molecular cascades for MF-LTP induction. Finally, we identify one major molecular mechanism underlying the emergence of MF-LTP.

Results

LTP and LTD Are Independent Processes at MF-PII Synapses. To examine the mechanisms underlying MF-LTP, we performed GC-PII paired whole-cell recordings in rat DG slices (Fig. 1). PIIs were identified by their low-input resistances, high-frequency discharges (>100 Hz) upon positive current injection (4), and characteristic axon distributions in the GC layer (Fig. 1*A*). In a subset of PIIs, PV expression was confirmed using antibody labeling (27 of 31 cells; Fig. 1*A*). Plasticity was induced at MF-PII synapses by applying a 30-Hz associative burst-frequency stimulation (aBFS) of presynaptic MFs paired with postsynaptic action potentials (APs) (3, 4) (Fig. S1*B*), thereby reproducing gamma activity (30–70 Hz) observed in the DG in vivo (1). Synaptic

Significance

During spatial learning, hippocampal fast-spiking inhibitory cells couple dynamically to excitatory principal cell (PC) assemblies that encode locations in the animal's environment. Repeated coactivation of highly active PC assemblies and fast-spiking interneurons strengthens their synaptic connections and promotes silencing of less active neurons, thereby stabilizing the active assembly. Here, we show that synaptic plasticity between excitatory dentate gyrus granule cells and fast-spiking interneurons requires coincident activation of postsynaptic Ca^{2+}-permeable AMPA and group I metabotropic glutamate receptors. Both jointly activate postsynaptic PKC to induce long-term synaptic plasticity. In the future, understanding the cellular and molecular mechanisms underlying synaptic plasticity between PCs and interneurons in vitro will enable us to study its role in memory formation in vivo.

Author contributions: T.H., A.K., and M.B. designed research; T.H. performed research; K.K. contributed new reagents/analytic tools; T.H., A.K., and M.B. analyzed data; and T.H., A.K., and M.B. wrote the paper.

The authors declare no conflict of interest.

This article is a PNAS Direct Submission.

Freely available online through the PNAS open access option.

[1]To whom correspondence should be addressed. Email: bartos@physiologie.uni-freiburg.de.

This article contains supporting information online at www.pnas.org/lookup/suppl/doi:10.1073/pnas.1409394111/-/DCSupplemental.

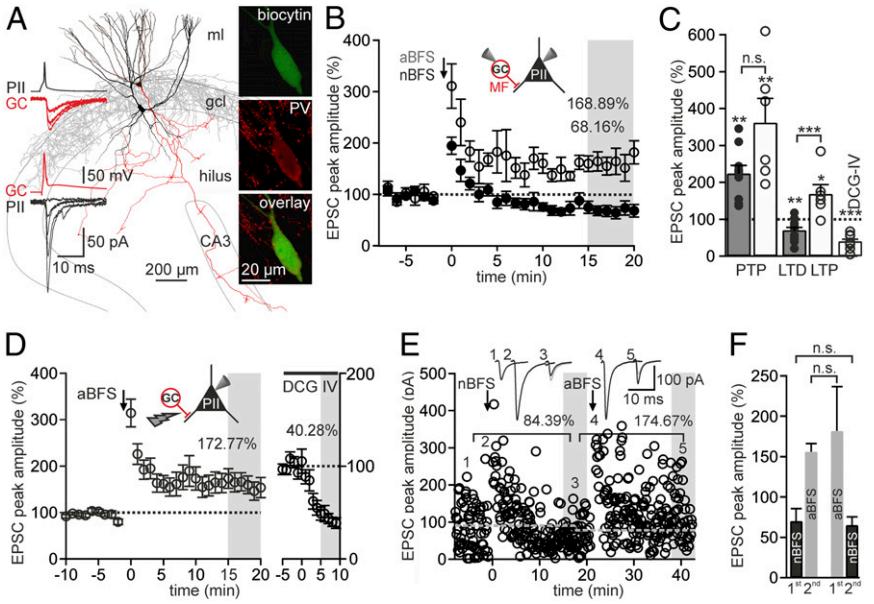

Fig. 1. Bidirectional long-term plasticity at GC-PII synapses. (*A*) Reconstruction of a biocytin-filled and bidirectionally coupled GC (red)-PII (black) pair (connectivity analysis is illustrated in Fig. S1*A*). (*Left Insets*) APs (*Upper* traces) in the PII or GC elicit unitary inhibitory postsynaptic currents and uEPSCs in the postsynaptic GC (red traces) or PII (black traces), respectively. Single traces are superimposed. (*Right*) Confocal images of biocytin labeling (*Top*), PV immunolabeling (*Middle*), and an overlay of both (*Bottom*) in a PII. (*B*) Plot shows the amplitude of uEPSCs after an aBFS (○, six pairs) or an nBFS (●, 10 pairs) applied at $t = 0$ min (arrow). Amplitudes were normalized to baseline and binned minute-wise. Long-term plasticity was measured 15–20 min after induction (gray area). Values indicate mean LTP or LTD. (*C*) PTP and LTP elicited by an nBFS (gray) and an aBFS (white). The rightmost bar shows the reduction of extracellularly evoked EPSCs by DCG-IV (○, individual experiments). (*D*) LTP was evoked by applying an aBFS to extracellularly stimulated MF inputs and PIIs (○, 25 PIIs). (*Right*) Sensitivity of MF-EPSCs to DCG-IV tested after LTP experiments (○, 11 PIIs). (*E*) uEPSC peak amplitudes recorded over time are shown for a representative GC-PII pair. An nBFS (first arrow) elicited LTD, and a subsequently applied aBFS (second arrow) elicited LTP. Dotted lines denote the preceding baseline. (*Insets*) Average uEPSCs at time points indicated by corresponding numbers. (*F*) Mean long-term plasticity elicited by an nBFS (black) and an aBFS (gray) when applied either first or second in a given pair. Bars represent six, three, three, and four pairs, respectively (left to right). $*P \leq 0.05$; $**P \leq 0.01$; $***P \leq 0.001$; n.s., not significant ($P > 0.05$). Bars and circles with lines denote mean ± SEM.

plasticity was quantified as the baseline normalized change in amplitude of unitary excitatory postsynaptic currents (uEPSCs) 15–20 min after the aBFS (Fig. 1 *B* and *C*). The aBFS resulted in a posttetanic potentiation (PTP; 361.66 ± 65.33% of baseline 0–30 s after the aBFS; $P = 0.007$), followed by LTP (168.89 ± 25.59% of baseline, six pairs; $P = 0.045$; Fig. 1*B*). Similar results were obtained when PIIs were intracellularly loaded with 100 µM spermine to compensate possible washout of polyamines (10) (Fig. S1*D*), confirming our previous investigations under an unperturbed intracellular PII milieu (3, 4). Similar results were also obtained with extracellularly evoked EPSCs (PTP: 373.35 ± 37.39%, LTP: 172.77 ± 22.95%, 25 PIIs; $P = 0.01$; Fig. 1*D*) blocked by (2S,2′R,3′R)-2-(2′,3′-Dicarboxycyclopropyl)glycine (DCG-IV; 0.5 µM, 40.28 ± 5.71%, 11 of 11 PIIs; Fig. 1*D* and Fig. S1*C*), confirming their MF-mediated nature. In contrast, a non-associative BFS (nBFS) protocol comprising GC activation while holding the PII at −70 or −90 mV (4) failed to induce LTP. The uEPSCs fell below baseline within 10 min after the nBFS, resulting in LTD (68.16 ± 9.66%, 10 pairs; $P = 0.01$; Fig. 1 *B* and *C*). Thus, LTP at MF-PII synapses depends on PII discharges.

To test whether LTD and LTP influence each other, we first applied an nBFS to GC-PII pairs to induce LTD and an aBFS 20 min thereafter (Fig. 1*E*). We observed a marked LTP which was indifferent to naive MF-PII synapses (156.02 ± 10.02% relative to the preceding LTD, three pairs; $P = 0.668$; Fig. 1*F*). Next, we changed the order of protocols and applied an nBFS 20 min after LTP induction. The resulting LTD was similar to naive terminals (65.29 ± 10.22% relative to preceding LTP, four pairs; $P = 0.824$; Fig. 1*E*). Thus, unlike bidirectional interference of LTD and LTP at CP-AMPARs containing GC-stratum lucidum interneuron contacts in CA3 (16), in which presynaptic mGluR7 is involved (16), DG MF-PII synapses seem to alternate between both forms of plasticity irrespective of their synaptic history.

MGluRs1α/5 Are Located in the Vicinity of MF-PII Synapses. MGluR1α is highly expressed in hippocampal SOM interneurons (15), and single-cell RT-PCR indicated the presence of mRNA encoding mGluRs1α/5 in CA1 fast-spiking interneurons (17). Whether mGluR1α is expressed in PV-PIIs remained controversial (14, 15). We therefore performed double-immunofluorescence labeling for PV and mGluR1α or for PV and mGluR5 (Fig. 2). Immunoreactivity for both mGluR types colocalized with PV^+ somata and dendrites in the hilus and GC layer (Fig. 2 *A* and *B*). However, labeling intensity was weaker for mGluR1α in PV^+ than in PV^-, presumably SOM^+, cells (15). Labeling of MGluRs1α/5 was also found in CA1 and CA3 PV^+ cells, suggesting that both receptors are expressed in PV-PIIs throughout the hippocampus (Fig. S2).

To confirm the expression of mGluRs1α/5 at basal PV^+ dendrites, the contact site of MFs (7), we performed double-labeling quantitative immunoelectron microscopy (18) (Fig. 2 *C*–*F*). When PV was visualized with immunogold and mGluR1α or mGluR5 was visualized with immunoperoxidase, we consistently found peroxidase reaction end product in hilar PV^+ dendritic profiles (Fig. 2 *C* and *D*). Conversely, when PV was labeled with immunoperoxidase and mGluR5 was labeled with immunogold, we consistently detected dense (12.44 ± 2.89 particles per square micrometer) immunogold labeling at membranes of PV^+ dendrites (Fig. 2*E*). We reconstructed PV^+ dendrites in three dimensions from serial ultrathin sections to examine mGluR5 distribution relative to asymmetrical synaptic contacts (seven dendritic segments; Fig. 2 *F* and *G*). The densest mGluR5 labeling was found at a distance of 0–60 nm from the edges of postsynaptic densities (PSDs; 23.4% of all particles), with few particles within PSDs (2.65%) (19) and a rapid decline of particles at distances of 60–300 nm, consistent with a perisynaptic location (15) (Fig. 2*G*). Membrane-associated immunogold particles labeling mGluR1α were seen in PV^+ dendrites near asymmetrical synapses, but their density was too sparse to be quantified. Thus, mGluRs1α/5 are expressed in DG PV-PIIs near putative MF synapses, suggesting that their activation by glutamate spills over during burst activity of GCs (1, 20).

MGluR1/5 Activation Is Needed but Not Sufficient for MF-LTP. To test the requirement of mGluRs1/5 for Hebbian MF-LTP induction, we applied an aBFS to GC-PII pairs in the presence of 2-Methyl-6-(phenylethynyl)pyridine hydrochloride (MPEP; 10 µM) or LY367385 (100 µM), which are selective antagonists of mGluR5 and mGluR1α, respectively (Fig. 3). In the presence of MPEP, a substantial PTP (344.19 ± 55.67% of baseline; $P = 0.046$) was followed by LTD instead of LTP (72.64 ± 10.2% of baseline, five

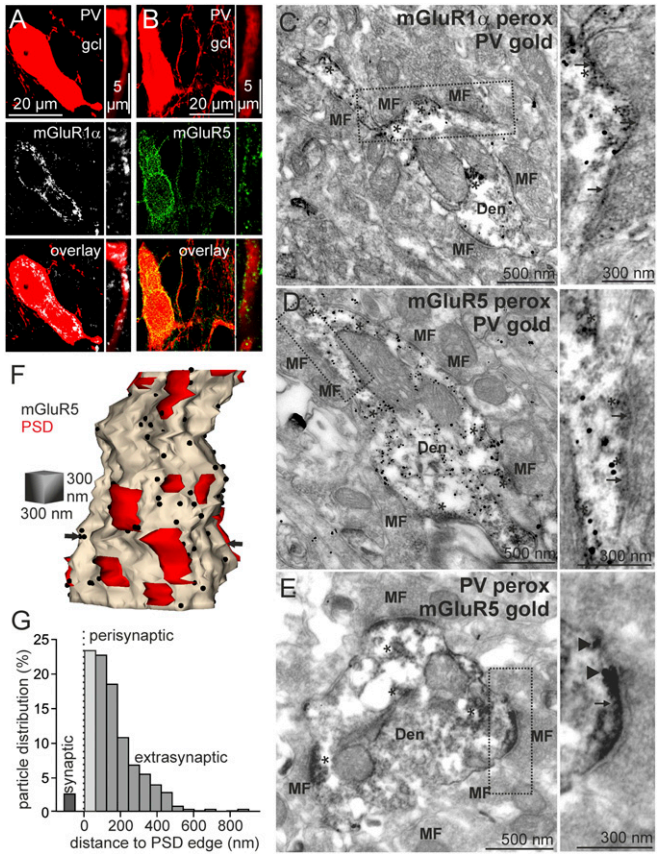

Fig. 2. PV-PIIs express mGluR1α and mGluR5. Confocal images of the DG showing immunofluorescent labeling for PV (red), mGluR1α (*A*, white), and mGluR5 (*B*, green) in somata (*Left*) and basal dendrites (*Right*). gcl, granule cell layer. Electron micrographs show dendritic profiles in the DG hilus with immunogold labeling of PV and immunoperoxidase labeling of mGluR1α (*C*, asterisks) and mGluR5 (*D*, asterisks). (*C* and *D*, *Right*) Regions indicated by dashed lines are shown. Note that islets of peroxidase reaction product (asterisks) are located close to asymmetrical, putative MF synapses (arrows). (*E*) Electron micrograph shows immunoreactivity for mGluR5 (*Right*; immunogold, arrowheads) in a PV^+ dendrite (*Left*; peroxidase reaction end product, asterisks). (*F*) Three-dimensional reconstruction of a PV^+ dendrite from 42 consecutive ultrathin sections showing peri- and extrasynaptic location of mGluR5 immunogold labeling (black dots) relative to PSDs (red areas) of asymmetrical synapses. Arrows point to the plane of the section shown in *E*. (*G*) Distribution of mGluR5 immunoparticles (n = 453) on PV^+ basal dendrites (n = 7) relative to the edges of the nearest PSD of an asymmetrical synapse. Bin size = 60 nm.

pairs; $P = 0.044$; Fig. 3*A*). A loss of LTP was also obtained with LY367385 (83.79 ± 11.07% of baseline, five pairs; $P = 0.63$; Fig. 3*A*) or with the coapplication of both antagonists (89.25 ± 3.23% of baseline, four pairs; $P = 0.13$; Fig. 3 *B* and *E* and Fig. S3*A*). To confirm that synapses would have shown plasticity in the absence of blockers, we washed out the antagonists for >20 min and applied a second aBFS in the same GC-PII pair (Fig. 3*B*). MF-LTP after washout was not different from naive synapses (198.57 ± 36.76%, four pairs tested; $P = 0.512$; Fig. 3*E*). Thus, preventing mGluR1 or mGluR5 activation blocks Hebbian MF-LTP.

Is activation of mGluRs1/5 sufficient to induce MF-LTP? We bath-applied the mGluRs1/5 agonist (S)-3,5-dihydroxyphenylglycine (DHPG; 100 µM) for 10 min and recorded extracellularly evoked MF-EPSCs in PIIs. EPSC amplitudes were reversibly reduced (Fig. 3*C*). Similar results were obtained when DHPG was paired with PII burst discharges at 30 Hz (Fig. S3 *D*, *F*, and *G*), indicating that mGluRs1/5 without CP-AMPAR activation did not induce LTP. Moreover, Hebbian MF-LTP could not be boosted further in the presence of DHPG (143.15 ± 21.17%, four PIIs; $P = 0.975$; Fig. S3*C*), suggesting that DHPG cannot supersede or occlude endogenous activation of mGluRs1/5. Finally, we asked whether mGluRs1/5 may influence MF-LTD by applying an nBFS in the presence of DHPG (Fig. 3*D*). Unlike control pairs, uEPSC amplitudes declined back to but not below baseline (106.88 ± 5.98%, seven pairs; $P = 0.22$; Fig. 3*E*), showing that activation of mGluRs1/5 prevented MF-LTD ($P = 0.008$). Similar results were obtained when 100 µM DHPG was transiently applied during the nBFS, indicating that mGluR activation blocks MF-LTD induction rather than its maintenance over time (Fig. S3 *E* and *G*).

In summary, group I mGluRs are required but not sufficient for MF-LTP. By supporting LTP and preventing LTD, mGluRs1/5 may act as a switch setting MF-PII synapses into a "readiness mode" for synaptic potentiation.

Major Contribution of CP-AMPARs and mGluRs1/5 to Synaptic Ca^{2+} Signaling in PII Dendrites. MF-LTP requires a postsynaptic Ca^{2+} rise (3), which could be evoked by CP-AMPARs (4), voltage-dependent Ca^{2+} channels (VDCCs) (21), or mGluRs1/5-mediated Ca^{2+} signals (22). To test their impact on MF-LTP, we first dissected their contribution to Ca^{2+} signals in PII dendrites by 2P imaging (Fig. 4). PIIs were intracellularly loaded with the Ca^{2+} indicator Fluo-5F (Invitrogen) and with Alexa Fluor 594 (Invitrogen). EPSCs were evoked at basal PII dendrites by extracellular stimulation of MFs, imaged at the dendrite, and recorded at the PII soma (Fig. 4*A*). Focal dendritic Ca^{2+} transients had a half-width of 6.2 ± 0.18 µm (Fig. S4*D*) similar to neocortical interneurons (23).

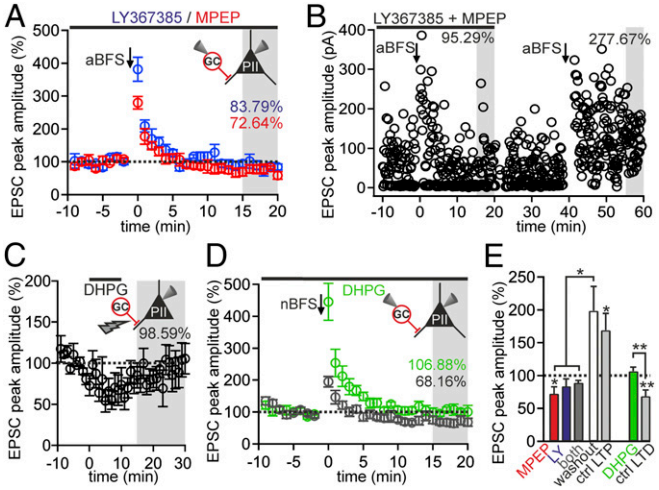

Fig. 3. Influence of group I mGluRs on long-term plasticity at MF-PII synapses. (*A*) aBFS applied to GC-PII pairs induces PTP, followed by LTD in the presence of either LY367385 (blue ○, five pairs) or MPEP (red ○, five pairs) to block mGluR1α or mGluR5, respectively. The horizontal bar indicates the time of LY367385 or MPEP bath application. (*B*) Individual uEPSCs are plotted against time during mGluR1α and mGluR5 blockade. The aBFS (first arrow) applied to a GC-PII pair induced PTP but no LTP. After washout of the antagonists, a second aBFS (second arrow) reliably evoked LTP in the same pair. (*C*) Summary graph illustrates the effect of the group I mGluR agonist DHPG (100 µM) on MF-evoked EPSCs (○, four PIIs). Note the reversible depression of MF-EPSCs and the lack of LTP. (*D*) Summary graph shows the effect of the nonassociative induction protocol (nBFS) on uEPSC amplitude in controls (black ○, 10 pairs) and in the presence of DHPG (5 µM; green ○, seven pairs). LTD induced by an nBFS was abolished by group I mGluR activation with DHPG. (*E*) Bar graphs summarize the effect of blockers of mGluRs1/5 on LTP at MF-PII synapses (*Left* group) and the influence of DHPG on LTD (*Right* group) in comparison to the washout of blockers of mGluRs1/5 (white bar, *Left* group only) and to control pairs (light gray bars). *$P \leq 0.05$; **$P \leq 0.01$. Bars and circles with lines denote mean ± SEM. LY, LY367385.

We positioned a line scan traversing the center of the putative postsynaptic location to compare Ca^{2+} rises evoked by a single burst of MF stimulation (nBFS), a single burst of the LTP induction protocol (aBFS), and a burst of somatically evoked back-propagating APs (25 spikes, 30 Hz; Fig. 4*B*). Signal amplitudes were stable throughout recordings and were neither affected by indicator saturation, as verified with the low-affinity Ca^{2+} indicator Fluo-4FF (Invitrogen; Figs. S4*C* and S5*J*), nor influenced by washout of intracellular polyamines (Fig. S5*I*). MF-mediated Ca^{2+} rises [44.15 ± 5.63% peak fluorescence change (ΔG/R), 28 PIIs; Fig. 4 *B* and *C*, red] were 2.6-fold larger than signals induced by spikes via VDCCs (16.82 ± 2.8%ΔG/R, 28 PIIs; P = 0.001; Fig. 4 *B* and *C*, blue) and only smaller than the ones evoked by the aBFS by a factor of 0.8 (57.95 ± 7.99% ΔG/R, 28 PIIs; P = 0.001; Fig. 4 *B* and *C*, black). Thus, the relevant Ca^{2+} sources for MF-LTP are postsynaptic receptors.

Next, we determined the relative contribution of ionotropic and metabotropic GluRs by measuring synaptically evoked Ca^{2+} signals in the presence of AP5, LY367385/MPEP, 6-Cyano-7-nitroquinoxaline-2,3-dione (CNQX), or the specific CP-AMPAR blocker 1-Naphthyl acetyl spermine trihydrochloride (NASPM) (Fig. 4*D* and Fig. S5*D*). Consistent with low expression of NMDARs in PIIs and their dispensability in MF-LTP (4), AP5 reduced synaptic Ca^{2+} signals moderately to 65.72 ± 6.27% of controls (11 PIIs; P = 0.002; Fig. 4*D*). CNQX or NASPM markedly diminished Ca^{2+} transients to 35.62 ± 7.03% (10 PIIs; P = 0.004) and 33.68 ± 3.95% (four PIIs; P = 0.051), respectively, in line with the requirement of CP-AMPARs for MF-LTP induction (4) (Fig. S1 *E* and *F*). Coapplication of LY367385/MPEP diminished synaptic Ca^{2+} signals to 48.81 ± 4.86% of control (eight PIIs; P = 0.001; Fig. 4*D*). This effect was enhanced when AMPARs and mGluRs were blocked simultaneously (13.77 ± 3.16% of control, nine PIIs; Fig. 4*D*). Finally, Ca^{2+} transients were almost entirely abolished by additional NMDAR blockade (3.22 ± 0.72% of control, six PIIs; Fig. 4*D*). Thus, CP-AMPARs and mGluRs1/5 mediate most of the Ca^{2+} influx at MF-PII contacts.

Two major mGluRs1/5-operated Ca^{2+} sources have been implicated in O/A interneuron LTP: internal Ca^{2+} stores (24) and cation-permeable transient receptor potential channels (TRPCs) (22). We examined their role in MF-LTP by loading PIIs with the Ca^{2+}-sensitive dye Oregon Green BAPTA-1 [1,2-bis(o-aminoethyl ether)-N,N,N′,N′-tetraacetic acid-1] (OGB-1) and puff-applied DHPG (100 μM for 20–100 ms) to basal PII dendrites (Fig. 4*E*). Delayed long-lasting Ca^{2+} transients were elicited (3.54 ± 0.49 s, stimulus onset to peak; nine PIIs; Fig. 4*F*) propagating from the dendrite toward the soma. They were markedly reduced by either MPEP or LY367385 (to 18.2 ± 7.45% and 6.38 ± 1.97% of control response integral, respectively; four PIIs each; Fig. 4 *F* and *G*). Each antagonist blocked >80% of the DHPG-evoked signal, and coapplication of both had no added effect (4.36 ± 0.94% of control; Fig. 4*G*), implying convergence of mGluR1 and mGluR5 on a common signaling cascade. Bath application of the TRPC and T-type VDCC blocker SKF96365 hydrochloride (SKF; 30 μM) and depletion of intracellular Ca^{2+}

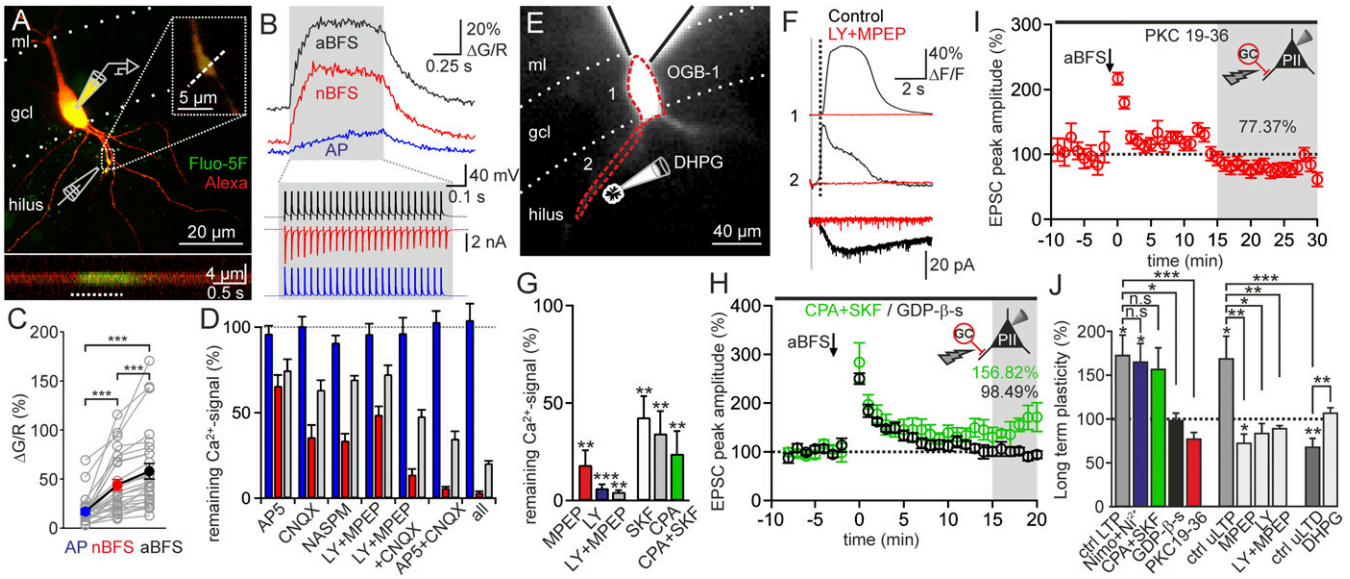

Fig. 4. Ca^{2+} signals required for LTP induction arise from CP-AMPARs. (*A*) Image stack of a PII filled with Fluo-5F (green) and Alexa Fluor 594 (red). EPSCs were evoked by extracellular stimulation. (*Upper Inset*) Region of interest (ROI) in which a line scan was positioned to detect synaptically evoked Ca^{2+} signals (Fig. S4). (*Lower Inset*) Line scan measurement at the same dendrite during an aBFS (white dotted line). (*B*, *Upper*) Traces of Ca^{2+} signals elicited by a burst of APs (25 APs at 30 Hz, blue), a burst of MF-EPSCs (nBFS, red), and a single burst of the MF-LTP induction protocol (aBFS, black). (B, *Lower*) Corresponding traces of somatically recorded signals. (*C*) Summary of the peak fluorescence (ΔG/R) induced by the three protocols (APs, nBFS, and aBFS). Individual experiments [○ connected by lines (gray)] and means (28 PIIs) (colored ● connected by a line) are shown. (*D*) Bars summarize AP- (blue), nBFS- (red), and aBFS-induced (gray) Ca^{2+} signals after bath application of AP5, CNQX, NASPM, LY, and MPEP or combinations of blockers normalized to their respective controls. Note that the AP-mediated Ca^{2+} signals (blue) were unaffected by blockers. Bar sets represent averages from 11, 10, 4, 8, 9, 11, and 6 PIIs, respectively (left to right). (*E*) Epifluorescence image of a PII filled with OGB-1. DHPG (100 μM) was puff-applied to the basal dendrite, and fluorescence signals were acquired in ROIs indicated by red dashed lines. ml, molecular layer. (*F*, *Upper*) Superimposed traces of Ca^{2+} signals elicited by a DHPG puff (20–100 ms, vertical gray bar) before (black) and after LY and MPEP (red) coapplication to the bath. (*F*, *Lower*) Traces of corresponding somatically recorded currents. The dotted line indicates the steepest rise of dendritic Ca^{2+} signals. (*G*) Bar graphs summarize the remaining DHPG-evoked Ca^{2+} signals normalized to controls in presence of MPEP, LY, SKF, and CPA. Means from four, four, two, six, four, and five PIIs, respectively (left to right), are shown. (*H*) Changes in EPSC amplitude after an aBFS (arrow) in the presence of CPA and SKF (green ○, four PIIs) and after intracellular loading of PIIs with GDP-β-s (black ○, seven PIIs). (*I*) PIIs dialyzed with the PKC blocker PKC 19-36 (red ○, nine PIIs) do not express MF-LTP. (*J*) Magnitude of long-term plasticity elicited by an aBFS (*Left* and *Center* groups of bars) and by an nBFS (*Right* group of bars) in the presence of all agents tested (25, 5, 4, 7, 4, 6, 5, 5, 4, 10, and 7 PIIs, respectively (left to right). Unitary LTP/LTD (uLTP/uLTD) depicts GC-PII pairs. *$P \leq 0.05$; **$P \leq 0.01$; ***$P \leq 0.001$; n.s., $P > 0.05$. Bars and circles with lines represent mean ± SEM.

stores with cyclopiazonic acid (CPA; 30 μM) significantly reduced DHPG-evoked Ca^{2+} signals (SKF: 42.68 ± 10.87% of control, six PIIs; $P = 0.003$ and CPA: 34.47 ± 11.4% of control, four PIIs; $P = 0.01$; Fig. 4*G*), and coapplication of both blockers drastically attenuated them (24.0 ± 11.02% of control, five PIIs; $P = 0.002$; Fig. 4*G*). However, MF-LTP was unaltered in the presence of both drugs (156.82 ± 24.35% of baseline, four PIIs; $P = 0.73$; Fig. 4*H*). Similarly, blockade of L-, R-, and T-type VDCCs (21) with nimodipine (10 μM) and Ni^{2+} (50 μM) left LTP unchanged (164.72 ± 21.33%; $P = 0.66$; Fig. S3*B*), consistent with their low overall contribution to aBFS-evoked Ca^{2+} signals (Fig. S5*H*). Thus, mGluR-evoked Ca^{2+} signals provide a reliable readout for mGluR activation during an aBFS but are themselves dispensable for LTP induction.

MF-LTP Requires PKC Activation by Group I mGluR-Mediated G Protein Signaling. MGluRs could contribute to MF-LTP via G protein-activated cascades. Indeed, aBFS protocols failed to induce MF-LTP when PIIs were dialyzed with the nonhydrolyzable GDP analog GDP-β-s (0.5 mM, 98.49 ± 8.13% of baseline, seven PIIs; $P = 0.8$; Fig. 4*H*). A plausible target of G protein-coupled molecular cascades is PKC. We therefore examined its role in synaptic plasticity by intracellular loading of PIIs with the inactivating PKC pseudosubstrate PKC 19-36 (10 μM). The aBFS failed to evoke LTP (77.37 ± 7.28% of baseline, nine PIIs; $P = 0.074$; Fig. 4*I*). Thus, mGluR-driven PKC activation via G proteins seems to be required for MF-LTP.

Differential Voltage-Dependent Modulation of Ca^{2+}-Permeable AMPAR- and mGluRs1/5-Mediated Signals. What is the functional role of PII APs in MF-LTP? Recent investigations in CA1 O-LM cells showed a voltage dependence of group I mGluR-mediated signals (22). To test whether this property applies to DG PIIs, we determined the relation between mGluRs1/5-mediated Ca^{2+} rises induced by DHPG puffs and the PII membrane holding potential (ΔF/V; Fig. 5*A*). Consistent with a voltage dependence, the largest Ca^{2+} inflow was evoked at −40 mV near PII spike threshold (V_{thres}; −38 ± 1.0 mV, 20 PIIs) but declined at more depolarized values (Fig. 5*B*). This ΔF/V relationship, however, raised the question of whether overshooting APs will facilitate or reduce mGluR signaling during LTP induction. To address this question, we first tested whether summation of Ca^{2+} signals from MF-EPSCs (nBFS) and postsynaptic APs was linear, reduced, or enhanced during an aBFS. We defined the linearity index of Ca^{2+} signals as the ratio between the sum of nBFS- and spike burst-induced Ca^{2+} transients and the ones induced by the aBFS. It was 94.42 ± 1.96% (28 PIIs; $P = 0.01$), showing a sublinear summation of MF- and spike-mediated Ca^{2+} transients during the aBFS, which may be explained by inward rectification of CP-AMPARs (4, 22). Indeed, after AMPAR blockade with CNQX, sublinearity was abolished (109.1 ± 7.12%, eight PIIs; $P = 0.016$; Fig. 5*D*) and changed to mild supralinearity with additional block of NMDARs (111.73 ± 3.41%, six PIIs; $P = 0.024$; Fig. 5 *C* and *D*). To test whether supralinearity was mGluRs1/5-dependent, we added LY367385 and MPEP to the bath, which resulted in a drop of the linearity index back to 91.24 ± 2.52% (six PIIs; $P = 0.006$; Fig. 5 *C* and *D*), implying a facilitating effect of APs on mGluR activity (25).

In summary, CP-AMPARs are negatively modulated by PII spikes, as indicated by sublinear Ca^{2+} signal summation, whereas mGluRs are positively modulated, as shown by their supralinearity. Accordingly, boosting of signaling of mGluRs1/5 via APs is a plausible switch enabling MF-LTP induction.

Discussion

Our results demonstrate that Hebbian LTP at MF-PII synapses is induced by a signaling cascade involving postsynaptic group I mGluR-released G proteins and CP-AMPAR–mediated Ca^{2+} rise, which jointly activate PKC. First, we show that mGluRs1/5

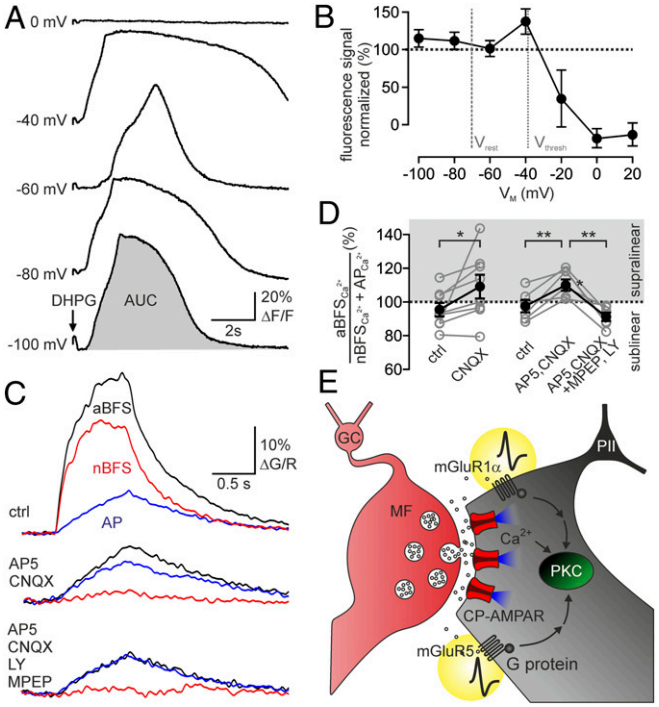

Fig. 5. Group I mGluR-mediated signals are enhanced by PII activity. (*A*) Traces represent individual Ca^{2+} signals induced by DHPG puffs (100 μM) to PII dendrites at different holding potentials (V_M). (*B*) Areas under the curve (AUC) of Ca^{2+} signals (●, six PIIs) were plotted against PII V_M normalized to the mean AUC across holding potentials. Note a peak in the ΔF/V plot between the PII membrane resting (V_{rest}) and V_{thres} potentials. (*C*) Ca^{2+} traces evoked by bursts of EPSCs (nBFS, red), a burst of back-propagating APs (blue), and the associative pairing protocol (aBFS, black) in control (ctrl) conditions (*Top*), after blockade of AMPARs and NMDARs (*Middle*), and after additional blockade of mGluRs1/5 (*Bottom*). (*D*) Ratio between the Ca^{2+} signal induced by the aBFS ($aBFS_{Ca}{}^{2+}$) and the summed Ca^{2+} signals evoked by the AP burst ($AP_{Ca}{}^{2+}$) and EPSCs ($nBFS_{Ca}{}^{2+}$). A value of 100% indicates that Ca^{2+} transients during the aBFS are exactly the sum of AP- and EPSC-mediated Ca^{2+} signals. Ca^{2+} signals summate sublinear in controls (*Left* recordings) and supralinear in the presence of CNQX and CNQX plus AP5 (*Right* recordings) leaving an isolated mGluRs1/5- and AP-mediated signal. (Right recordings) Ca^{2+} transients go back to sublinearity after additional blockade of mGluRs1/5. Individual recordings (gray ○ connected by lines) and means (● connected by lines) from eight (left recordings) and six (right recordings) PIIs, respectively, are shown. (*E*) Schematic illustration of the major cellular and molecular mechanisms involved in MF-LTP induction. Glutamate is released from MFs and binds at postsynaptic CP-AMPARs and extrasynaptic mGluRs1/5. Postsynaptic APs facilitate mGluR signaling (details are provided in main text). Strong CP-AMPAR–mediated Ca^{2+} signals (blue) and G protein-mediated signals cooperatively activate PKC in the PII. $*P \leq 0.05$; $**P \leq 0.01$. Circles with lines represent mean ± SEM.

are localized peri- and extrasynaptically at MF-PII synapses. This localization fits with perisynaptic expression of mGluRs1/5 in hippocampal PCs and non-PCs (19) and previous single-cell RT-PCR studies in fast-spiking interneurons (17, but see refs. 14, 15). Second, we show that Ca^{2+} signals needed for LTP induction are largely mediated by CP-AMPARs and less by NMDARs, mGluRs1/5, VDCCs, or Ca^{2+} release from internal stores (Fig. 4 and Fig. S5). This fits with our finding that CP-AMPARs (Fig. S1), but not NMDARs (4), VDCCs, or mGluR-mediated Ca^{2+} signals, are required for MF-LTP (Fig. 4*J*). Plasticity is blocked when PIIs are loaded with BAPTA, but not with EGTA (3), indicating the need for strong focal postsynaptic Ca^{2+} rises to drive LTP induction. This need can be met by CP-AMPAR–mediated, but not by small NMDAR-mediated, Ca^{2+} signals and perisynaptic locations of mGluRs and VDCCs (21)

(Figs. 2 and 4). Third, we provide evidence that a major mechanism underlying LTP induction involves PKC (Fig. 4*I*), which is activated by Ca^{2+} and G protein signaling via phospholipase C and diacylglycerol (26). Our results are in contrast to results found with CA1 PIIs, where mGluR-evoked endocannabinoid release induces LTD (27), a mechanism that is absent at MF-PII synapses, very likely due to the lack of presynaptic cannabinoid receptors (28).

Pharmacological activation of mGluRs1/5 alone or paired with postsynaptic APs did not induce LTP. However, blocking mGluRs1/5 results in a loss of MF-LTP (Fig. 3), and activation of both receptors abolished MF-LTD, implying that mGluRs1/5 recruitment gates PIIs into a readiness mode to promote LTP induction. This gating is likely caused by spike-mediated boosting of mGluR1/5 activation (22, 25). Indeed, ΔF/V of mGluRs1/5-evoked Ca^{2+} signals showed a peak near V_{thres} (Fig. 5*B*). Although ΔF/V showed a decline at suprathreshold potentials, mGuR1/5-driven Ca^{2+} signaling was supralinear during the aBFS, indicating that mGuR1/5 activation was facilitated. Thus, our results support the view that voltage-dependent facilitation of signaling of mGluRs1/5 cooperates with focal CP-AMPAR–gated Ca^{2+} signals to mobilize PKC, and thereby induce MF-PII LTP (26) (Fig. 5*E*). Removal of any of the components of this cascade results in a loss of LTP. Our findings are in contrast to recent investigations showing that activation of mGluRs1/5 alone induced LTP in stratum oriens interneurons and LTD at glutamatergic inputs onto distal dendrites of fast-spiking interneurons in CA1 (12). This fact highlights the diversity of mechanisms underlying synaptic plasticity among cortical GABAergic cell types (13, 29).

How does MF-PII LTP influence DG network function? The DG is thought to transform a rich entorhinal input into a sparse code for CA3. If GC activity is too low to recruit PIIs reliably, MF-LTD will emerge and make the DG network more responsive for entorhinal inputs. In contrast, strong inputs will recruit GCs to discharge at high frequency (20), thereby resulting in activation of mGluRs1/5 by glutamate spillover and PII recruitment. Repeated activation of these GCs and associated PIIs will strengthen their coupling by MF-LTP, increasing the suppression of competing less excited GCs. An assembly of highly excited GCs and coupled PIIs will arise, reflecting the emergence of a memory trace in the DG.

Materials and Methods

Electrophysiology. Whole-cell recordings from rat hippocampal slices were performed as previously described (4) (*SI Materials and Methods*). All experiments involving animals were approved by the Regierungspräsidium Freiburg (license no. X10-18S and G11/19). We used two plasticity induction protocols: (*i*) nBFS (a 30-Hz burst of 25 APs in the presynaptic GC, repeated 12 times every 3 s with the postsynaptic PII voltage-clamped at −70 mV) and (*ii*) aBFS (same as for the nBFS but paired with postsynaptic APs with a 1- to 3-ms delay in the current-clamped PII) (Fig. S1*B*).

Ca^{2+} Imaging. Dendritic Ca^{2+} signals were measured using a 2P galvoscanning microscope (Femto 2D; Femtonics) with a mode-locked Ti:sapphire laser (Chameleon Ultra II; Coherent) tuned to 800 nm and analyzed with Mes software (Femtonics). Signals were quantified as the peak of green fluorescence change (ΔG) normalized to the red channel (R_0). Slow DHPG-evoked Ca^{2+} signals in OGB-1 (100 μM)–filled PIIs were acquired with a CCD-camera (Neuroccd; RedShirt Imaging) and quantified as the integral of green fluorescent change (ΔF) divided by OGB-1 baseline fluorescence (F_0). Details are provided in *SI Materials and Methods*.

Immunohistochemistry. Immunohistochemistry was performed as described (4, 18). We used antibodies against PV (Swant) and mGluR1α or mGluR5 (both from Frontier Institute). Details are provided in *SI Materials and Methods*.

Data Analysis and Statistics. Details are provided in *SI Materials and Methods*.

ACKNOWLEDGMENTS. We thank K. Winterhalter, K. Semmler, N. Callies, S. Nestel, and B. Joch for technical support and Drs. I. Vida, J. C. Lacaille, J. F. Sauer, B. Fakler, J. Bischofberger, and D. Althoff for reading earlier versions of the manuscript. This work was funded by the Deutsche Forschungsgemeinschaft: Grant BA 1582/2-1 (to M.B.), Project FOR2143 (to M.B.), and Project BIOSS-2 A6 (to A.K.); and by the Volkswagen Foundation (M.B.), Schram Foundation (M.B.), BrainLinks-BrainTools, Cluster of Excellence funded by the Deutsche Forschungsgemeinschaft (grant number EXC 1086) (M.B.), and MotiVate Program of Freiburg University Clinics (T.H.).

1. Leutgeb JK, Leutgeb S, Moser M-B, Moser EI (2007) Pattern separation in the dentate gyrus and CA3 of the hippocampus. *Science* 315(5814):961–966.
2. Dupret D, O'Neill J, Csicsvari J (2013) Dynamic reconfiguration of hippocampal interneuron circuits during spatial learning. *Neuron* 78(1):166–180.
3. Alle H, Jonas P, Geiger JRP (2001) PTP and LTP at a hippocampal mossy fiber-interneuron synapse. *Proc Natl Acad Sci USA* 98(25):14708–14713.
4. Sambandan S, Sauer J-F, Vida I, Bartos M (2010) Associative plasticity at excitatory synapses facilitates recruitment of fast-spiking interneurons in the dentate gyrus. *J Neurosci* 30(35):11826–11837.
5. Donato F, Rompani SB, Caroni P (2013) Parvalbumin-expressing basket-cell network plasticity induced by experience regulates adult learning. *Nature* 504(7479):272–276.
6. Le Roux N, Cabezas C, Böhm UL, Poncer JC (2013) Input-specific learning rules at excitatory synapses onto hippocampal parvalbumin-expressing interneurons. *J Physiol* 591(Pt 7):1809–1822.
7. Geiger JR, Lübke J, Roth A, Frotscher M, Jonas P (1997) Submillisecond AMPA receptor-mediated signaling at a principal neuron-interneuron synapse. *Neuron* 18(6):1009–1023.
8. Lei S, McBain CJ (2002) Distinct NMDA receptors provide differential modes of transmission at mossy fiber-interneuron synapses. *Neuron* 33(6):921–933.
9. Perez Y, Morin F, Lacaille JC (2001) A hebbian form of long-term potentiation dependent on mGluR1a in hippocampal inhibitory interneurons. *Proc Natl Acad Sci USA* 98(16):9401–9406.
10. Lamsa KP, Heeroma JH, Somogyi P, Rusakov DA, Kullmann DM (2007) Anti-Hebbian long-term potentiation in the hippocampal feedback inhibitory circuit. *Science* 315(5816): 1262–1266.
11. Galván EJ, Calixto E, Barrionuevo G (2008) Bidirectional Hebbian plasticity at hippocampal mossy fiber synapses on CA3 interneurons. *J Neurosci* 28(52):14042–14055.
12. Camiré O, Topolnik L (2014) Dendritic calcium nonlinearities switch the direction of synaptic plasticity in fast-spiking interneurons. *J Neurosci* 34(11):3864–3877.
13. Nicoll RA, Schmitz D (2005) Synaptic plasticity at hippocampal mossy fibre synapses. *Nat Rev Neurosci* 6(11):863–876.
14. Kerner JA, Standaert DG, Penney JB, Jr, Young AB, Landwehrmeyer GB (1997) Expression of group one metabotropic glutamate receptor subunit mRNAs in neurochemically identified neurons in the rat neostriatum, neocortex, and hippocampus. *Brain Res Mol Brain Res* 48(2):259–269.
15. Baude A, et al. (1993) The metabotropic glutamate receptor (mGluR1 alpha) is concentrated at perisynaptic membrane of neuronal subpopulations as detected by immunogold reaction. *Neuron* 11(4):771–787.
16. Pelkey KA, Topolnik L, Yuan X-Q, Lacaille J-C, McBain CJ (2008) State-dependent cAMP sensitivity of presynaptic function underlies metaplasticity in a hippocampal feedforward inhibitory circuit. *Neuron* 60(6):980–987.
17. van Hooft JA, Giuffrida R, Blatow M, Monyer H (2000) Differential expression of group I metabotropic glutamate receptors in functionally distinct hippocampal interneurons. *J Neurosci* 20(10):3544–3551.
18. Kulik A, et al. (2002) Distinct localization of GABA(B) receptors relative to synaptic sites in the rat cerebellum and ventrobasal thalamus. *Eur J Neurosci* 15(2):291–307.
19. Lujan R, Nusser Z, Roberts JD, Shigemoto R, Somogyi P (1996) Perisynaptic location of metabotropic glutamate receptors mGluR1 and mGluR5 on dendrites and dendritic spines in the rat hippocampus. *Eur J Neurosci* 8(7):1488–1500.
20. Pernía-Andrade AJ, Jonas P (2014) Theta-gamma-modulated synaptic currents in hippocampal granule cells in vivo define a mechanism for network oscillations. *Neuron* 81(1):140–152.
21. Vinet J, Sík A (2006) Expression pattern of voltage-dependent calcium channel subunits in hippocampal inhibitory neurons in mice. *Neuroscience* 143(1):189–212.
22. Topolnik L, Congar P, Lacaille J-C (2005) Differential regulation of metabotropic glutamate receptor- and AMPA receptor-mediated dendritic Ca2+ signals by presynaptic and postsynaptic activity in hippocampal interneurons. *J Neurosci* 25(4):990–1001.
23. Goldberg JH, Tamas G, Aronov D, Yuste R (2003) Calcium microdomains in aspiny dendrites. *Neuron* 40(4):807–821.
24. Topolnik L, Azzi M, Morin F, Kougioumoutzakis A, Lacaille J-C (2006) mGluR1/5 subtype-specific calcium signalling and induction of long-term potentiation in rat hippocampal oriens/alveus interneurones. *J Physiol* 575:115–131.
25. Ohana L, Barchad O, Parnas I, Parnas H (2006) The metabotropic glutamate G-protein-coupled receptors mGluR3 and mGluR1a are voltage-sensitive. *J Biol Chem* 281(34): 24204–24215.
26. Oancea E, Meyer T (1998) Protein kinase C as a molecular machine for decoding calcium and diacylglycerol signals. *Cell* 95(3):307–318.
27. Péterfi Z, et al. (2012) Endocannabinoid-mediated long-term depression of afferent excitatory synapses in hippocampal pyramidal cells and GABAergic interneurons. *J Neurosci* 32(41):14448–14463.
28. Katona I, et al. (2006) Molecular composition of the endocannabinoid system at glutamatergic synapses. *J Neurosci* 26(21):5628–5637.
29. Liu Y-C, Cheng J-K, Lien C-C (2014) Rapid dynamic changes of dendritic inhibition in the dentate gyrus by presynaptic activity patterns. *J Neurosci* 34(4):1344–1357.